Structural differences in the FAD-binding pockets and lid loops of mammalian CRY1 and CRY2 for isoform-selective regulation

Simon Miller[a,1], Ashutosh Srivastava[a,b,1], Yoshiko Nagai[a], Yoshiki Aikawa[a], Florence Tama[a,c,d], and Tsuyoshi Hirota[a,2]

[a]Institute of Transformative Bio-Molecules, Nagoya University, 464-8601 Nagoya, Japan; [b]Biological Engineering Discipline, Indian Institute of Technology Gandhinagar, 382355 Gandhinagar, India; [c]Graduate School of Science, Department of Physics, Nagoya University, 464-8601 Nagoya, Japan; and [d]RIKEN–Center for Computational Science, Kobe 650-0047, Japan

Edited by Joseph S. Takahashi, The University of Texas Southwestern Medical Center, Dallas, TX, and approved May 21, 2021 (received for review December 20, 2020)

The circadian clock is a biological timekeeper that operates through transcription–translation feedback loops in mammals. Cryptochrome 1 (CRY1) and Cryptochrome 2 (CRY2) are highly conserved core clock components having redundant and distinct functions. We recently identified the CRY1- and CRY2-selective compounds KL101 and TH301, respectively, which provide useful tools for the exploration of isoform-selective CRY regulation. However, intrinsic differences in the compound-binding FAD (flavin adenine dinucleotide) pockets between CRY1 and CRY2 are not well understood, partly because of nonoptimal properties of previously reported apo form structures in this particular region constituted by almost identical sequences. Here, we show unliganded CRY1 and CRY2 crystal structures with well-defined electron densities that are largely free of crystal contacts at the FAD pocket and nearby lid loop. We revealed conformational isomerism in key residues. In particular, CRY1 W399 and corresponding CRY2 W417 in the FAD pocket had distinct conformations ("out" for CRY1 and "in" for CRY2) by interacting with the lid loop residues CRY1 Q407 and CRY2 F424, respectively, resulting in different overall lid loop structures. Molecular dynamics simulations supported that these conformations were energetically favorable to each isoform. Isoform-selective compounds KL101 and TH301 preferred intrinsic "out" and "in" conformations of the tryptophan residue in CRY1 and CRY2, respectively, while the nonselective compound KL001 fit to both conformations. Mutations of lid loop residues designed to perturb their isoform-specific interaction with the tryptophan resulted in reversed responses of CRY1 and CRY2 to KL101 and TH301. We propose that these intrinsic structural differences of CRY1 and CRY2 can be targeted for isoform-selective regulation.

circadian clock | cryptochromes | X-ray crystallography | molecular dynamics simulation | small-molecule modulators

The circadian clock controls daily rhythms of physiological processes including sleep/wake routines, hormone secretion, body temperature, and metabolic regulation. This biological clock operates at molecular and cellular levels throughout the organism with ~24-h periodicity. The transcription factors CLOCK and BMAL1 form a heterodimer that activates transcription of *Period* (*Per1* and *Per2*) and *Cryptochrome* (*Cry1* and *Cry2*) genes (1). PER and CRY proteins form complexes in the cytoplasm and together with other regulatory proteins, translocate to the nucleus (2) where they close a negative feedback loop by interacting with CLOCK-BMAL1 and inhibiting their own transcription (3). Complex formation of CRY1 or CRY2 with the F-box protein FBXL3 induces proteasomal degradation, while FBXL21 causes stabilization (4–8). CRY degradation results in the reactivation of CLOCK-BMAL1, enabling the circadian clock to initiate a new 24-h cycle. Although CRY1 and CRY2 have overlapping functions in clock regulation, there is evidence to suggest that they also have distinct mechanisms of action in output pathways (9, 10).

Deletion of *Cry1* and *Cry2* genes results in period shortening and lengthening in mice, respectively (11). In humans, a CRY1 splice variant that lacks exon 11 has been associated with familial delayed sleep phase disorder with late-phase sleep/wake times, leading to lengthening of the clock period (12). A CRY2 A260T missense mutation results in increased FBXL3 interaction, and thus enhanced degradation, which is associated with familial advanced sleep phase and shortening of the period (13). In addition to influencing sleep timing, CRYs also regulate metabolic processes such as hormone-induced gluconeogenesis (14, 15) and brown adipose tissue differentiation (16). Therefore, small-molecule compounds that can regulate CRY function are highly sought after for potential therapeutic treatment, in addition to molecular tools to facilitate understanding of circadian clock mechanisms. Since the discovery of KL001 that stabilizes both CRY1 and CRY2 (17), multiple derivatives have been developed (18–21) and applied against diabetes (20, 21) and glioblastoma (22).

Crystal structure determination of the photolyase homology regions (PHRs) (*SI Appendix*, Fig. S1*A*) of CRY1-apo (23),

Significance

CRY1 and CRY2 regulate circadian rhythms, and their dysfunction has been associated with many diseases. Since they have not only similar but also independent functions, understanding of intrinsic differences between these highly similar proteins is required. Here, we determined CRY1 and CRY2 static and dynamic structures that exhibited conformational isomerism in their ligand-binding FAD pockets and neighboring lid loops, allowing mechanistic insight into structural features specific to each isoform. Structure-guided mutations supported important roles of interactions between a key "gatekeeper" tryptophan residue in the FAD pocket and lid loop residues in determining the effects of isoform-selective compounds. Our results provide insight into how near-identical ligand-binding pockets can intrinsically regulate compound selectivity through unique interactions with neighboring structural elements.

Author contributions: S.M. and T.H. designed research; S.M., A.S., Y.N., and Y.A. performed research; S.M., A.S., F.T., and T.H. analyzed data; T.H. supervised the project and secured funding; and S.M. and T.H. wrote the paper.

The authors declare no competing interest.

This article is a PNAS Direct Submission.

[1]S.M. and A.S. contributed equally to this work.

[2]To whom correspondence may be addressed. Email: thirota@itbm.nagoya-u.ac.jp.

This article contains supporting information online at https://www.pnas.org/lookup/suppl/doi:10.1073/pnas.2026191118/-/DCSupplemental.

Published June 25, 2021.

CRY2-apo (24), and CRY2-KL001 complex (25) provided important insights into structural features of mammalian CRYs and also paved the way for an array of compound-bound CRY structures. Isoform-selective targeting of CRY1 and CRY2 has proven difficult due to very high sequence identity, particularly in the FAD pocket where KL001 locates (25) and competes with the C-terminal tail of FBXL3 (24). On the other hand, by using phenotypic screening of circadian period modulators, we recently identified compounds KL101 and KL201 that are selective against CRY1, and TH301 that shows preference against CRY2 (16, 26). Although these compounds bind to the FAD pocket in the PHR, they require the CRY C-terminal tail (CCT) (*SI Appendix*, Fig. S1*A*) for their selective effects. Unlike the high sequence similarity of the PHRs between CRY1 and CRY2, the CCTs are diverged in their sequences, and swapping of CCT results in no response to KL101 and TH301 in both CRY1 and CRY2 (16). Because CCT swapping does not reverse compound responses, it is possible that CCTs work in combination with PHRs, especially FAD pocket residues that directly interact with compounds, to determine compound selectivity. In support of this hypothesis, crystal structures of CRY1(PHR) bound to KL101 and KL201, and CRY2(PHR) bound to TH301 revealed conformational differences among conserved residues in their FAD pockets and lid loops (16, 26, 27) (Table 1 and *SI Appendix*, Table S1). However, it was not known whether these differences were induced by compounds or intrinsic to CRY isoforms because the conformations of critical residues were ambiguous in previously reported apo structures of CRY1 and CRY2, due to poorly defined electron density and/or steric restraints caused by crystal packing. In order to better understand structural features underlying CRY isoform selectivity, more precise structures of the FAD pockets and lid loops in apo CRY1 and CRY2 isoforms are required.

In this study, we solved the X-ray crystal structures of the PHR of mouse CRY1 and CRY2 with well-defined electron density in the FAD pocket and lid loop. Based on these structures and also solution dynamics studied through molecular dynamics (MD) simulations, we identified isoform-specific conformations of CRY1 W399 and CRY2 W417 in the FAD pocket and their interactions with CRY1 Q407 and CRY2 F424 in the lid loop, respectively. Structure-guided mutations supported the role of interactions between the lid loop and FAD pocket, as well as the CCT, in the selectivity of KL101 and TH301. These differential conformations between CRY1 and CRY2 may provide a rationale into isoform-selective regulation.

Results

Crystal Structures of Apo CRY1 and CRY2. The FAD pocket, located in the C-terminal α-helical domain, is composed of 17 residues that interact with compounds. Nine residues (Q289, W292, R293, H355, H359, L385, I392, W399, and L400 in mouse CRY1) display conformational differences among previously reported CRY crystal structures (Table 1 and *SI Appendix*, Table S1), while the remaining residues are stable and show no or only small differences. In particular, CRY1 Q289, H355, I392, W399, and L400 (corresponding to CRY2 Q307, H373, V410, W417, and L418) show large conformational variation between CRY1-KL101 and CRY2-TH301 and can directly interact with the compounds (16). In contrast, CRY1 R293 and L385 typically adopt very similar conformations with corresponding CRY2 R311 and L403 and are only associated with indirect conformational changes upon the binding of certain compounds, unrelated to isoform selectivity (*SI Appendix*, Table S1). CRY1 I392 (CRY2 V410) is the only variant residue in the FAD pocket between CRY1 and CRY2, but CRY1 I392V and CRY2 V410I mutations do not affect KL101 and TH301 selectivity (16). CRY1 Q289 (CRY2 Q307) is a particularly flexible residue and prone to disorder in multiple CRY structures, in which a specific rotamer often cannot be determined, although it engages in a compound-induced interaction with TH301 but not KL101.

Table 1. Conformational isomerism of CRY1 and CRY2 FAD-binding pocket residues

		W292 (W310)	H355 (H373)	H359 (H377)	W399 (W417)		L400(L418)
PDB ID code	Protein compound	χ1 (°)	χ1 (°)	χ1 (°)	χ1 (°)	χ2 (°)	χ1 (°)
4I6E	CRY2-apo	−83	70	−63	−175	−74	−100
4I6G	CRY2-FAD	−85	−180	−85	−179	−69	71
4MLP	CRY2-KL001	−88	−76	−73	−178	85	177
6KX8	CRY2-TH301	−86	−84	−94	−174	92	−176
7EJ9	CRY2-TH301	−87	−80	−175	180	89	−170
7D0N	CRY2-apo	−86	−83	−52	−164	86	−97
4K0R	CRY1-apo	−94	−68	−62	168	58	−109
5T5X	CRY1-apo	−155	−84	−72	174	−73	−62
6KX4	CRY1-apo	−155	−87 [72]	−79	−178	−75	−62
6KX5	CRY1-KL044	−82	−86	−75	176	−70	−100
6KX6	CRY1-KL101	−89	−172 [−105]	−72	−167	−60	−63
6KX7	CRY1-TH301	−87	−91	−92	173	82	69
6LUE	CRY1-KL201	−88	176	−66	−178	−63	−80
7DLI	CRY1-KL001	−88	−76	−89	−166	−65	n/a
7D0M	CRY1-PG4	−82	170	−90	178	−79	62

Parentheses denote CRY2 residues. Square brackets denote alternative conformers. χ-values represent minus (−60°), trans (180°), and plus (+60°). Orange and yellow indicate a sizeable χ-angle change of ±30° or more, compared with CRY2-apo (7D0N) or CRY1-PG4 (7D0M), due to a direct interaction with the bound compound (orange) and indirect conformational changes upon compound binding (yellow). Gray signifies a conformation potentially caused by crystal packing or unexplained density in close proximity to the residue. Cyan denotes atomic coordinates that are not (fully) supported by electron density. Red and blue characters represent gatekeeper tryptophan "in" and "out" conformations, respectively. n/a indicates that the side chain was truncated at the β-carbon due to poor electron density.

Therefore, we paid particular attention to H355, W399, L400, and also neighboring W292 and H359 as candidate residues that potentially have influence on compound binding. The lid loop, consisting of residues 405 to 412 in CRY1 (equivalent to 423 to 430 in CRY2), is adjacent to the FAD pocket and can potentially interact with and regulate residues in the FAD pocket. In most of the reported CRY structures, lid loop conformations were affected by crystal packing interactions and/or unreliable coordinates for lid loop residues that have been modeled into poorly defined or absent electron density, making their comparison difficult.

We determined the structures of mouse CRY2-apo (Fig. 1*A*) at a resolution of 2.8 Å (Protein Data Bank [PDB] ID code 7D0N) and mouse CRY1-PG4 (CRY1 with a bound precipitant/cryoprotectant tetraethylene glycol [PG4] in the FAD pocket) (Fig. 2*A*) at 1.95 Å (PDB ID code 7D0M) (*SI Appendix*, Table S2). Both structures formed canonical photolyase folds consistent with previously determined structures (23, 24, 28, 16), comprising an N-terminal α/β-domain and a C-terminal α-helical domain, connected by an extended linker region. Well-defined electron density was present for the secondary structure elements that encapsulated the FAD pocket, enabling accurate model building and structural interpretation of CRY2-apo, although the N terminus of the α/β-domain, parts of the linker region, and several loops in the α-helical domain exhibited disorder, thus influencing R_{free} and R_{work} values (*SI Appendix*, Table S2). The higher-resolution CRY1-PG4 structure had clearly interpretable overall density with minimal chain breaks and excellent geometric criteria (*SI Appendix*, Table S2). Below, we describe CRY2 and CRY1 structures with a focus on variable FAD pocket and lid loop residues that have sufficient electron density to support their conformations.

Structure and Dynamics of the CRY2 FAD Pocket and Lid Loop. A notable feature of our CRY2-apo structure (7D0N) (Fig. 1*A*) was well-resolved electron density for W417 and the N-terminal portion of the lid loop (residues 423 to 425) (Fig. 1*B*). W417 adopted an "in" conformation (ξ3-carbon orientated down) and formed a stacking interaction with F424 in the lid loop, which in turn formed a sulfur–π interaction with C420. This W417–F424–C420 (π–π–sulfur–π) interaction is unique among CRY crystal structures and appears to stabilize both the N-terminal portion of the lid loop and the "in" conformation of W417. Residues 423 to 427 in the lid loop were free from crystal packing (*SI Appendix*, Fig. S1*B*), suggesting that this conformation could have formed intrinsically. In contrast, residues 428 to 430 were juxtaposed to a crystallographic symmetry-related molecule (*SI Appendix*, Fig. S1*B*), which likely imposed conformational restraint on the C-terminal part of the lid loop. Among the other residues in the FAD pocket, H373 and L418 are typically flexible with varying conformations (Table 1). The electron density of H373 enabled the side chain to be modeled in the highest occupancy conformation, despite some flexibility, and we observed sufficient electron density for the L418 conformation to be traced to a single rotamer (Fig. 1*B*). W310 adopted an "up" position and formed a stacking interaction with Y168 in the α6-helix, and H377 had good density with a stable rotamer.

In order to provide further insight into intrinsic and dynamic conformations of these residues, we performed MD simulations. W417 exhibited a predominant "in" conformation similar to the crystal structure, with minor "out" and "middle" conformations during MD simulations (Fig. 1 *C*, *Left* and *SI Appendix*, Fig. S1*C*). The lid loop residue F424 predominantly formed a π–aryl stacking interaction with W417 "in", like the crystal structure (Fig. 1 *D*, *Left*), while a minor conformation of F424 formed a T-shaped stacking or hydrophobic interaction with W417 "in" (Fig. 1 *D*, *Right*). The conformation of C420 remained stable throughout the simulation (Fig. 1 *C*, *Right*). The W417–F424–C420 interaction in the simulation correlated to a more stable structure in lid loop residues 423 to 427, compared with the flexibility observed in residues 428 to 430, reflected by lower RMSF (root mean square fluctuation) values (Fig. 1*E*). The interaction energies calculated for W417–F424 and F424–C420 from MD simulation trajectories were −4.02 and −2.87 kcal/mol, respectively, showing energetically favorable interactions. These data support a preferential W417 "in" conformation in CRY2-apo and show that F424 remains in proximity to W417 (*SI Appendix*, Fig. S1*D*). Regarding other FAD pocket residues of interest (Fig. 1*F*), W310 maintained an "up" conformation similar to the CRY2-apo crystal structure in a major population of frames, H373 showed a high level of flexibility, H377 adopted a reasonably stable conformation similar to the crystal structure, and L418 displayed some flexibility but with a major conformation close to the crystal structure. Overall, conformations of these residues in the crystal structure agreed well with the conformations observed in major populations during MD simulations.

Structure and Dynamics of the CRY1 FAD Pocket and Lid Loop. In the CRY1-PG4 (7D0M) crystal structure (Fig. 2*A*), the FAD pocket residue W399 adopted an "out" conformation (Fig. 2*B*). In this configuration, W399 formed N–H aryl and H-bond interactions with Q407 in the lid loop, which are supported by clearly defined electron density for both W399 and the N-terminal portion of the lid loop (Fig. 2*B*). Crystal packing was largely absent in proximity to the lid loop (*SI Appendix*, Fig. S2*A*), allowing a high degree of conformational freedom and potentially providing a window into an intrinsic lid loop structure. Regarding other FAD pocket residues corresponding to CRY2 W310, H373, H377, and L418, CRY1 W292 adopted an "up" conformation, although the bound PG4 molecule in the FAD pocket could have influenced the orientation of this residue. H355 and H359 adopted stable conformations with well-resolved electron density (Fig. 2*B*) due to a crystal packing–mediated interaction where, together with W399, they engaged in hydrogen bonds with D203 in a crystallographic symmetry–related molecule (D203-symmetry) (*SI Appendix*, Fig. S2*B*). L400 adopted a stable conformation orientated toward the center of the FAD pocket.

In order to characterize the dynamic conformations of these residues in the absence of PG4 and the symmetry-related molecule, we performed MD simulations by removing PG4. W399 was found to be very stable in the "out" conformation perhaps due to an interaction with Q407, which also displayed a stable conformation in close proximity to W399 throughout the simulation (Fig. 2*C*). The calculated interaction energy between W399 and Q407 was −6.76 kcal/mol, showing an energetically favorable interaction that correlated to the stable conformation of the lid loop N-terminal region in the simulation with relatively low RMSF values (Fig. 2*D*). W292 adopted both "up" and "down" conformations (Fig. 2*E*). H355 showed two main conformations, one resembling the CRY1-PG4 crystal structure and the other similar to the alternate conformer in the previously published CRY1-apo structure 6KX4. H359 and L400 were both very stable with conformations similar to the CRY1-PG4 crystal structure. Overall, the conformations of these residues in the crystal structure correlated to the predominant orientations in MD simulations, suggesting minimal effect of PG4 on the conformations of H355, H359, W399, and L400 in CRY1-PG4 with the exception of W292. No effect of PG4 or its derivatives on CRY1(PHR) stabilization in a thermal shift assay supported its negligible interaction with CRY1 (Fig. 2*F*). Taken together, we consider CRY1-PG4 to be representative of an apo structure, and all comparisons hereafter excluded the consideration of PG4.

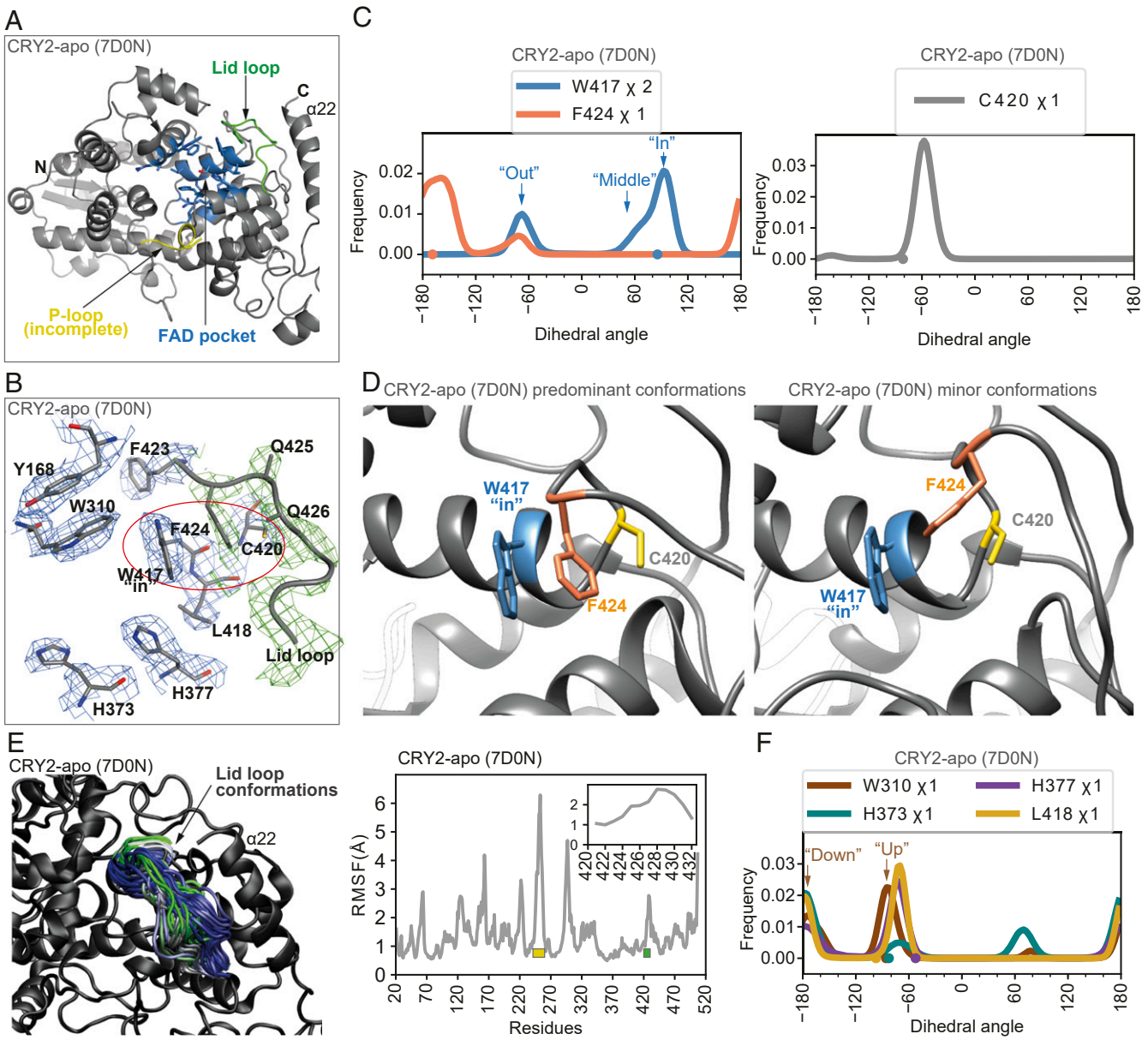

Fig. 1. Crystal structure and MD of CRY2-apo. (*A*) Overall structure of CRY2-apo (7D0N). FAD pocket residues, the lid loop, and the partially ordered P-loop are colored blue, green, and yellow, respectively. (*B*) Electron density of FAD pocket and lid loop residues. 2mFo-DFc electron density (basic electron density map, blue mesh) was contoured to 1.1 σ and is shown for FAD pocket residues (W310, H373, H377, W417, L418) as well as Y168, C420, and F423 (lid loop N terminus). mFo-DFc omit map electron density (green mesh) was contoured to 2.2 σ and is shown for lid loop residues 424 to 430. The density supports W417–F424 π–aryl stacking and F424–C420 sulfur–π interactions (red oval). (*C*) χ-dihedral angle distributions of residues at the W417–lid loop interface in MD simulations. Colored dots show the values for the conformations of corresponding residues in the crystal structure. (*D*) Structural representation of major and minor F424 conformations of MD simulations in *C*. (*E*) Lid loop flexibility during MD simulations. *Left* shows snapshots of lid loop conformations during MD simulations. The frames were extracted from the 1.5-μs concatenated trajectory at the interval of 20 ns and are colored in the green–gray–blue spectrum based on the time step in the combined trajectory of three simulations (500 ns each). *Right* shows the root mean square fluctuation of all residues (yellow and green bars indicate the positions of the P-loop and lid loop, respectively). The N-terminal region of the lid loop displayed considerably less flexibility than the C-terminal region (*Inset* in *Right*). (*F*) χ-dihedral angle distributions of FAD pocket residues in MD simulations.

Another regulatory feature of CRY proteins is the P-loop (residues 231 to 247), which has been shown to regulate circadian rhythms via accumulating phosphorylation (29). The P-loop is very flexible and largely disordered in most CRY structures including CRY2-apo, inhibiting structural insights into potential mechanisms of action. A complete P-loop could be modeled into clearly interpretable electron density in CRY1-PG4 (*SI Appendix*, Fig. S2*C*). This was primarily due to multiple crystal packing interactions, including contacts with the secondary pocket loop (also complete) and the α22-helix in symmetry-related molecules (*SI Appendix*, Fig. S2*D*). R236 extended into the FAD pocket, potentially within interacting distance of H354, H355, the PG4 molecule, and D201 in a symmetry-related molecule (*SI Appendix*, Fig. S2 *C* and *D*). However, during the course of MD simulation, the P-loop showed considerable flexibility (Fig. 2 *D*, *Lower*, yellow region), and R236 exited the FAD pocket (*SI Appendix*, Fig. S2*E*), clearly suggesting that the P-loop conformation in CRY1-PG4 and the

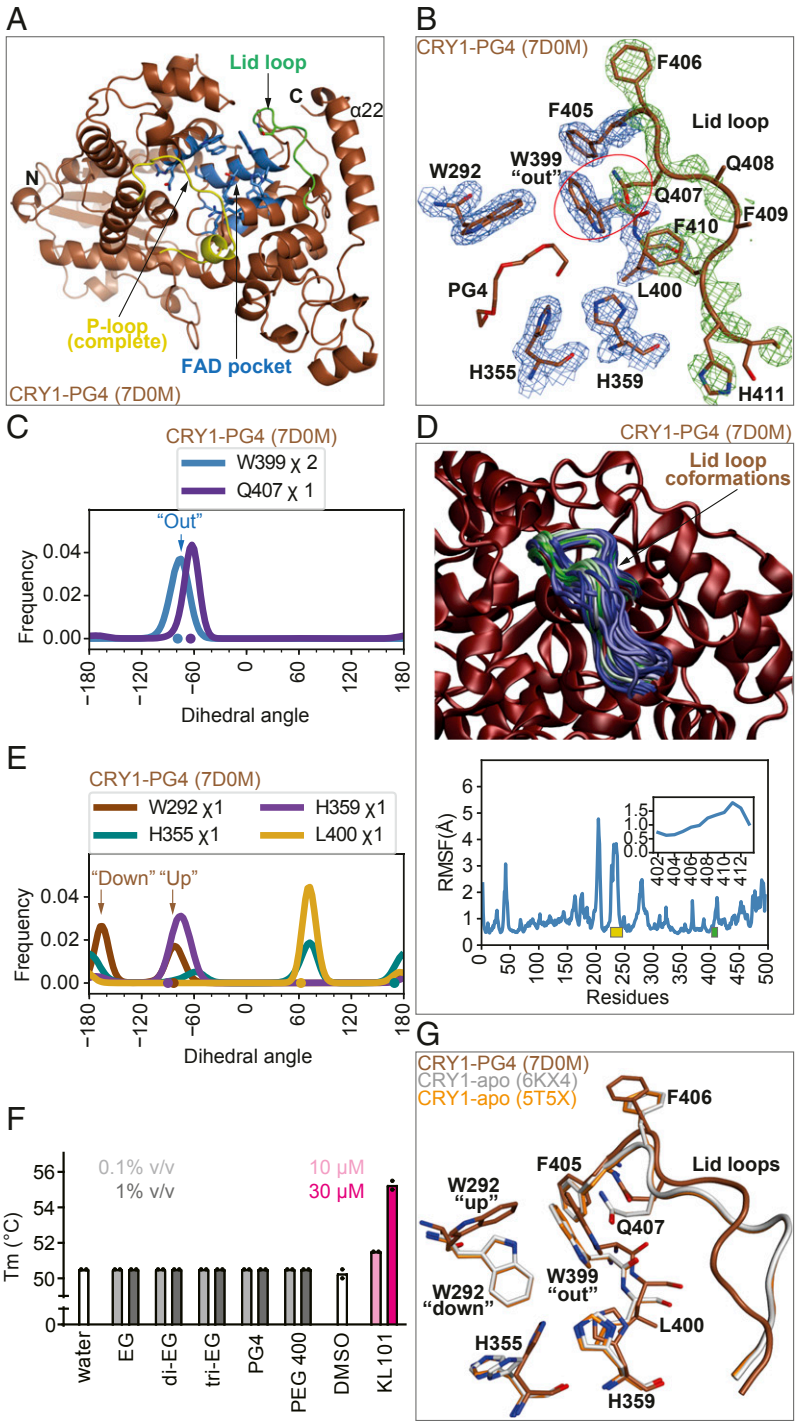

Fig. 2. Crystal structure and MD of CRY1-PG4. (*A*) Overall structure of CRY1-PG4 (7D0M). FAD pocket residues, the lid loop, and the complete P-loop are colored blue, green, and yellow, respectively. (*B*) Electron density of FAD pocket and lid loop residues. 2mFo-DFc electron density (basic electron density map, blue mesh) was contoured to 1.1 σ and is shown for FAD pocket residues (W292, H355, H359, W399, L400) and lid loop residue 405. mFo-DFc omit map electron density (green mesh) was contoured to 2.7 σ and is shown for lid loop residues 406 to 411. The density supports an N–H aryl interaction formed between W399 "out" and Q407 (red oval). PG4 was present in the crystallization buffer and cryoprotectant solution and located in the FAD pocket of the crystal structure. (*C*) χ-dihedral angle distributions of residues in the W399–lid loop interface in MD simulations. Colored dots show the values for the conformations of corresponding residues in the crystal structure. (*D*) Lid loop flexibility during MD simulations. *Upper* shows snapshots of lid loop conformations during the MD simulations. The frames were extracted from the 1.5-μs concatenated trajectory at the interval of 20 ns and are colored in the green–gray–blue spectrum based on the time step in the combined trajectory of three simulations (500 ns each). *Lower* shows the root mean square fluctuation of all residues (yellow and green bars indicate the positions of the P-loop and lid loop, respectively). The N-terminal region of the lid loop displayed considerably less flexibility than the C-terminal region (*Inset* in *Lower*). (*E*) χ-dihedral angle distributions of FAD pocket residues in MD simulations. (*F*) No interaction of PG4 or related molecules ethylene glycol (EG), diethylene glycol (di-EG), triethylene glycol (tri-EG), or polyethylene glycol (PEG) 400 with CRY1(PHR) in vitro. Denaturing temperatures of recombinant CRY1(PHR) in the presence of various polymers of ethylene glycol or the CRY1-selective compound KL101 as a positive control are shown. Dimethyl sulfoxide (DMSO) is a solvent of KL101. Compound interaction induced thermal stabilization. (*G*) Superposition of CRY1-PG4 (7D0M) with CRY1-apo 5T5X and 6KX4 crystal structures.

interaction of R236 with FAD pocket residues were an artifact of crystal packing.

The space group in which a crystal structure is determined can affect the conformations of residues or structural features, either through direct interactions or long-range indirect effects. In the previously published CRY1-apo structures 5T5X and 6KX4 (both crystallized in the P1 space group with almost identical structures), crystal packing of a symmetry-related molecule constrained the lid loop (*SI Appendix*, Fig. S3*A*), resulting in well-defined electron density due to the lack of flexibility. In contrast, CRY1-PG4 (space group $P2_12_12_1$) had far more conformational freedom around the lid loop (*SI Appendix*, Fig. S2*A*), yet despite these structural differences, CRY1-apo (5T5X and 6KX4) and CRY1-PG4 formed the same W399–Q407 interaction (Fig. 2*G*). We evaluated this interaction by looking at MD simulation data of 5T5X (30), which showed that the conformations of W399 and Q407 were stable (*SI Appendix*, Fig. S3*B*) and energetically favorable with an interaction energy of −6.72 kcal/mol. Together, these data suggest that CRY1 preferentially adopts a W399 "out" conformation and that an interaction with Q407 in the lid loop could stabilize this orientation.

A notable difference was observed for W292 among the two CRY1-apo and CRY1-PG4 crystal structures (Fig. 2*G*), which together with W399, form an upper boundary of the FAD pocket. The W292 "up" conformation in CRY1-PG4 facilitated a stacking interaction with Y150 in the α6-helix, which was largely free of crystal packing restraints (*SI Appendix*, Fig. S3*C*). In contrast, crystal packing in CRY1-apo (6KX4) induced conformational restraint of the α6-helix (*SI Appendix*, Fig. S3*D*). Consequently, Y150 encroached into a position that could cause a steric clash with an "up"-orientated W292, thus potentially inducing W292 to rotate "down". Accordingly, MD simulations showed that W292 adopted a "down" conformation with greater frequency in CRY1-apo (5T5X) (*SI Appendix*, Fig. S3*E*) than in CRY1-PG4 (Fig. 2*E*). However, the difference in the relative population of "up" and "down" conformations between CRY1-apo (5T5X) and CRY1-PG4 was small, suggesting that a W292–Y150 interaction could be transient. H355 adopted a completely different rotamer conformation in the CRY1-PG4 crystal structure, compared with CRY1-apo 6KX4 and 5T5X (Fig. 2*G*). Unlike in CRY1-PG4, H355 in CRY1-apo (5T5X) was unable to form a hydrogen bond with a symmetry-related molecule due to different crystal packing (*SI Appendix*, Fig. S3*F*). In MD simulations of CRY1-PG4 and CRY1-apo (5T5X), without the crystal packing effects, the H355 side chain orientations showed similar distributions (Fig. 2*E* and *SI Appendix*, Fig. S3*E*). The α22-helix in CRY1-PG4 was extended at the C-terminal region (residues 490 to 495) compared with CRY1-apo, due to crystal packing–induced stabilization. Because α22 is adjacent to the lid loop and the C-terminal extension formed hydrogen bonds with C402 (just prior to the lid loop) and also the electron-rich sulfur loop (*SI Appendix*, Fig. S3*G*), we evaluated the effect of this region on the conformations of the FAD pocket residues and Q407 by performing MD simulations of CRY1-PG4 with truncation after Q489. Truncation of the α22-extension increased flexibility of the C-terminal end (*SI Appendix*, Fig. S3*H*) but did not affect the conformations of the FAD pocket residues and Q407 (*SI Appendix*, Fig. S3*I*). Taken together, the crystallographic and MD simulation data show that the conformations of the FAD pocket and lid loop residue Q407 in the CRY1-PG4 crystal structure are energetically favorable and that overall differences compared with CRY1-apo structures (5T5X and 6KX4) can be explained by crystal packing interactions.

Nuances of CRY1 and CRY2 FAD Pockets and Lid Loops. Despite the very high sequence identity among residues in the FAD pockets and lid loops of CRY1 and CRY2, a number of structural differences were present between CRY1-PG4 and CRY2-apo (Fig. 3*A* and *SI Appendix*, Fig. S4*A*). Of particular interest was the differential orientation of CRY1 W399/CRY2 W417 (designated the gatekeeper tryptophan due to rotamer interactions with the lid loop): "out" orientation in CRY1 and "in" orientation in CRY2. This conformational isomerism correlated to distinct lid loop structures and interactions, where F424 and Q425 in CRY2 were rotated ∼180° around the main chain, relative to F406 and Q407 in CRY1, and structural differences pervaded until the C-terminal ends of the lid loops (Fig. 3*A* and *SI Appendix*, Fig. S4*A*). Other FAD pocket residues, CRY1 H355, H359, and L400 (CRY2 H373, H377, and L418, respectively) also displayed differences in conformation (Fig. 3*A* and *SI Appendix*, Fig. S4*A*). Together, we revealed a striking intrinsic difference in the conformations of the gatekeeper tryptophan and the lid loop, as well as the differential organization of several FAD pocket residues, which are specific to CRY isoforms.

The distinct gatekeeper conformations in CRY1-PG4 and CRY2-apo were highly conserved in crystal structures with bound compounds. CRY1 W399 "out" conformation was observed in complexes with the CRY1-selective compounds KL101 (6KX6) (Fig. 3*B*) and KL201 (6LUE) (*SI Appendix*, Fig. S4 *B*, *Left*). Q407 interacted with the gatekeeper in CRY2-KL201, but in CRY1-KL101, Q407 was truncated at the β-carbon in chain A and was not modeled in chain B because of weak lid loop electron density. We therefore modeled the side chain of Q407 in the CRY1-KL101 structure into a polder (omit) map, which clearly showed an interaction between Q407 and the gatekeeper (*SI Appendix*, Fig. S4*C*), similar to CRY1-PG4. Because the rest of the lid loop residues were disordered in the CRY1-KL101 crystal structure, we also superposed and inserted KL101 into the CRY1-PG4 structure (PG4 removed) and performed an MD simulation. W399 in CRY1-PG4 did not clash with KL101 and maintained an "out" conformation (*SI Appendix*, Fig. S4*D*) throughout the simulation (Fig. 3 *C*, *Left*). The interaction between W399 and Q407 was found to be stable with an interaction energy of −6.96 kcal/mol. These data demonstrated that the intrinsic W399–Q407 conformation in CRY1 was amenable to KL101 binding.

A CRY2 W417 "in" conformation was observed in complex with the CRY2-selective compound TH301 (6KX8) (*SI Appendix*, Fig. S4*E*). Compared with CRY2-apo (Fig. 3*A*), the positions of F424 and Q425 in CRY2-TH301 (6KX8) were inverted, likely due to a crystal packing effect where Q425 formed an H-bond with E214 in the neighboring chain of the crystallographic dimer, leading to its proximity to W417 instead of F424 (*SI Appendix*, Fig. S4*F*). To evaluate the effects of crystal packing on the lid loop, we determined a CRY2-TH301 structure at 2.60 Å (PDB ID code 7EJ9) (Fig. 3*B* and *SI Appendix*, Table S2) in a different space group to CRY2-TH301 (6KX8) by modifying the crystallization conditions. No crystal packing was present near the lid loop in the CRY2-TH301 (7EJ9) structure (*SI Appendix*, Fig. S5*A*), and the lid loop was largely disordered. This result supported that the inverted lid loop in CRY2-TH301 (6KX8) was an artifact of crystal packing. Well-defined electron density showed that the gatekeeper in CRY2-TH301 (7EJ9) adopted the same "in" conformation as CRY2-TH301 (6KX8) and CRY2-apo (Fig. 3*B* and *SI Appendix*, Fig. S5*B*). Other FAD pocket residues W310, H373, and L418 in CRY2-TH301 (7EJ9) also adopted similar conformations to CRY2-TH301 (6KX8), except H377 (*SI Appendix*, Fig. S5*C* and *Discussion*). Because the proper conformation of F424 was not obtained from CRY2-TH301 crystal structures (6KX8 and 7EJ9), we conducted superposition and insertion of TH301 into the CRY2-apo structure, followed by an MD simulation. W417 maintained an "in" conformation (*SI Appendix*, Fig. S4*D*) for the entire course of the simulation, with no minor populations of "out" or "middle" conformations (Fig. 3 *C*, *Right*). The interaction between W417 and F424 was found to be stable with an interaction energy of −4.00 kcal/mol, similar to CRY2-apo without modeled TH301. Together, these data indicated that the intrinsic W417–F424 conformation in CRY2 was

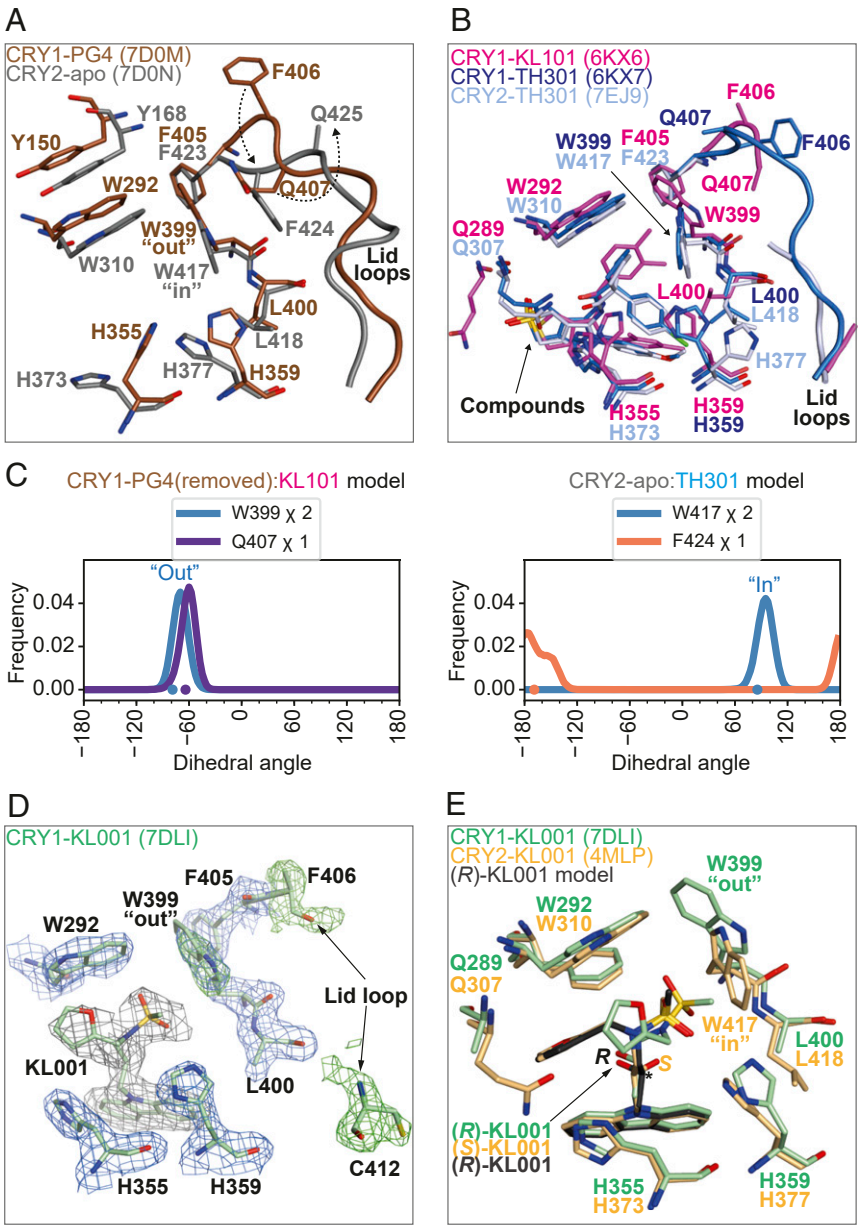

Fig. 3. Structural differences between CRY2 and CRY1. (*A*) Superposition of CRY2 7D0N (gray) and CRY1 7D0M (brown) structures. F424 and Q425 in CRY2 adopted opposite conformations to the corresponding F406 and Q407 residues in CRY1 (dashed arrows). The main chains of the CRY1 and CRY2 lid loops were rotated ∼180° relative to each other, resulting in the juxtaposition of different lid loop residues to CRY1 W399 and CRY2 W417, which adopted distinct "out" and "in" conformations, respectively. (*B*) Superposition of CRY1-KL101 6KX6 (magenta), CRY1-TH301 6KX7 (blue), and CRY2-TH301 7EJ9 (blue–white) structures. The CRY1-selective compound KL101 is accommodated by a W399 "out" conformation, like the CRY1-apo structure, and TH301 induces a stacking interaction with a CRY1 W399/CRY2 W417 "in" conformation, correlating to the CRY2-apo structure. (*C*) χ-dihedral angle distributions of the gatekeeper tryptophan W399 and lid loop Q407 in MD simulations of the CRY1-PG4(removed):KL101 model (*Left*) and the W417 and F424 in CRY2-apo:TH301 model (*Right*). Colored dots show the values of the conformations of corresponding residues in the crystal structures of CRY1-PG4 and CRY2-apo. (*D*) Electron density for FAD pocket and lid loop residues in the CRY1-KL001 complex (7DLI). 2mFo-DFc electron density (basic electron density map, blue mesh) was contoured to 1.1 σ and is shown for FAD pocket residues (W292, H355, H359, W399, L400) and the lid loop residue F405. mFo-DFc omit map electron density (green mesh) was contoured to 2.7 σ and is shown for W399 and lid loop residues 406 and 412. A polder (omit) map (gray mesh) was produced by omitting KL001 in the Phenix Polder Maps utility and is shown for KL001 with a contour level of 3.0 σ. Disordered lid loop residues 407 to 411 were not modeled in the structure. (*E*) Superposition of CRY1-KL001 7DLI (green) and CRY2-KL001 4MLP (light orange). The view was rotated 20° around the *y* axis compared with *D*. An *R*-configuration KL001 molecule (black) was modeled into the density of the CRY2-KL001 4MLP structure, refined in Refmac5, and superposed onto the CRY2-KL001 structure. The default (*S*)-KL001 and refined (*R*)-KL001 structures in CRY2-KL001 had very similar positional coordinates for the methansulfonamide moiety but a repositioned hydroxy group. The stereocenter of KL001 is indicated by a black asterisk.

amenable to TH301 binding and that W417 was more stabilized in an "in" conformation by this compound.

We further investigated intrinsic gatekeeper conformations by performing MD simulations starting with opposite orientations: CRY1-PG4 (PG4 removed) with W399 modeled "in" and CRY2-apo with W417 modeled "out". When CRY1-PG4 W399 was started from an artificial "in" position, it remained stable throughout a 300-ns simulation. The side chain of Q407 flipped

to interact with W399 "in" (*SI Appendix*, Fig. S5 *D*, *Top*), suggesting that CRY1 W399 can stably adopt an "in" conformation, while intrinsic W399 "out" is by far the predominant orientation among CRY1 structures (Table 1). The tolerated W399 "in" conformation in the simulation correlated to the CRY1-TH301 structure, where W399 adopted an "in" conformation similar to CRY2 (Fig. 3*B*), supporting a TH301-induced conformational change of the gatekeeper through a favorable stacking interaction with the cyclopentyl group of the compound. This TH301-induced CRY1 gatekeeper "in" conformation caused a lost interaction with Q407, which in combination with crystal packing (*SI Appendix*, Fig. S5*E*), resulted in a different lid loop conformation in CRY1-TH301 to CRY1-PG4 (Fig. 3 *A* and *B*).

In contrast, artificially modeled CRY2-apo W417 "out" induced steric clashes with W310 and F423 (*SI Appendix*, Fig. S5*F*) that resulted in W417 rotating to an "in" conformation after ~50 ns of MD simulation, and it remained in that conformation for the rest of the trajectory (*SI Appendix*, Fig. S5 *D*, *Middle* and *Bottom*). In combination with the loss of a stacking interaction between F424 and W417 "out", the steric clash between W417 "out" and F423 appeared to affect lid loop conformation because F424 and Q425 rotated to positions similar to CRY1 F406 and Q407. These data suggest that CRY2 W417 favored an "in" conformation, and rotation to an "out" conformation was not tolerated. Superposition of CRY2-apo with KL101 showed that a large steric clash would occur between CRY2 W417 "in" and the dimethylphenyl moiety of KL101 (*SI Appendix*, Fig. S5*G*). Taken together, intrinsic gatekeeper tryptophan conformations appear to interfere with compounds having opposite selectivity. The results also correlated to the high selectivity of KL101 for CRY1 and the moderate selectivity of TH301 for CRY2.

In order to obtain insight into whether conformational differences of the gatekeeper could accommodate isoform nonselective compounds, we determined the crystal structure of CRY1-KL001 at 2.2 Å (PDB ID code 7DLI) (*SI Appendix*, Table S2). The presence of three molecules in each asymmetric unit resulted in crystal packing differences in proximity to the FAD pockets and lid loops of the three protein chains. From structural comparisons with CRY1-PG4, we determined that chain A of CRY1-KL001 was the most similar (and potentially, the most biological) due to the least crystal packing restraints around the FAD pocket and lid loop. The carbazole moiety stably bound in the pocket with well-defined electron density, and the hydroxypropyl linker and the methansulfonamide showed a reasonably good fit to the electron density (Fig. 3*D*). In contrast, the furan moiety displayed flexibility and a potentially alternate conformation (*SI Appendix*, Fig. S5*H*). In CRY1-KL001, the compound had an *R* stereocenter, designated (*R*)-KL001, whereas in CRY2-KL001 (4MLP), an *S* stereocenter was built into the model, (*S*)-KL001 (Fig. 3*E*). Modeling the *R* form of KL001 into the CRY2-KL001 (4MLP) structure and its refinement revealed that the structure has bound *R* form and not *S* form. Because the compound used for crystallization was from a racemic mixture, the result suggested that (*R*)-KL001 was the active form. (*R*)-KL001 bound to both CRY1 and CRY2 pockets with a slight shift of the methansulfonamide to avoid a steric clash with CRY2 W417 "in", without affecting the original gatekeeper conformation (Fig. 3*E*). These data show that KL001 can bind to the FAD pockets of CRY1 and CRY2 with distinct gatekeeper "out" or "in" conformations, likely due to the small and flexible functional groups.

To further assess isoform-specific orientations of FAD pocket residues, we extended structural comparisons with other CRY PDB entries, except protein complexes. We found that the majority of mammalian CRY crystal structures exhibited CRY1 W399 "out" and CRY2 W417 "in" conformations (Table 1). Also, a trend emerged for a conformation of CRY1 H355 in CRY1-selective compound structures (*Discussion*). CRY1 L400 (CRY2 L418) showed a range of conformations and appears to function in affinity rather than selectivity. A W417 "in" conformation limits the range of motion of L418 in CRY2, due to steric overlap between the two residues. In CRY1 structures, W399 "out" enables more conformational freedom of L400, which forms hydrophobic, CH–π, and CH–Cl interactions in CRY1-KL101, CRY1-KL201, and CRY1-KL044 structures, respectively (Fig. 3*B* and *SI Appendix*, Fig. S4*B*). Q289 displayed considerable flexibility in several CRY structures but was stabilized by a compound-induced interaction in

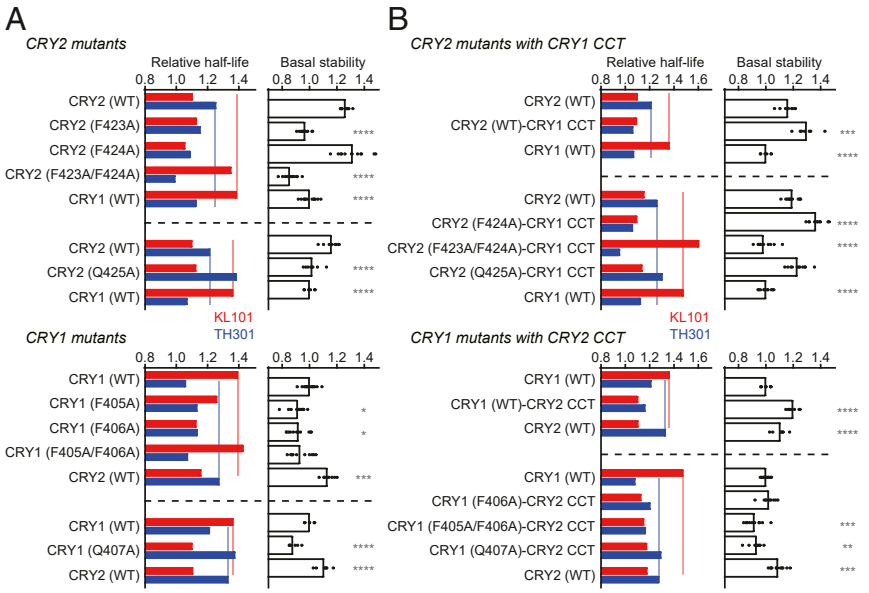

Fig. 4. Effects of CRY2 and CRY1 mutation on the responses against KL101 and TH301 in HEK293T cells. (*A* and *B*) The half-lives of CRY1-LUC, CRY2-LUC, and their mutants relative to LUC are plotted by setting a dimethyl sulfoxide (DMSO) control of each protein to 1 for each experiment (*SI Appendix*, Fig. S6) (mean of $n = 4$ to 6 biologically independent samples from two to three experiments), and values at 3.3 μM compound are shown (*Left*). Red and blue vertical lines represent half-lives of KL101-treated CRY1 (WT) and TH301-treated CRY2 (WT) in each set of experiments, respectively. Basal stability of each protein treated with DMSO is shown in *Right* by setting CRY1 stability to 1 (mean of $n = 8$ to 12). *$P < 0.05$; **$P < 0.01$; ***$P < 0.001$; ****$P < 0.0001$ relative to CRY2 (WT) for CRY2 mutants or to CRY1 (WT) for CRY1 mutants by one-way ANOVA followed by Tukey's multiple comparisons test.

CRY1-TH301 and CRY2-TH301 structures, influencing affinity but not selectivity (*SI Appendix*, Table S1). We further investigated the conformations of other FAD pocket residues that adopted diverse conformations in CRY structures, CRY1 R293, L385, and I392 (corresponding to CRY2 R311, L403, and V410), but found no correlation with compound selectivity (*SI Appendix*, Table S1). Overall, the most notable association with compound selectivity was observed for the gatekeeper residue.

Distinct Lid Loop Interactions with the Gatekeeper Affect KL101 and TH301 Selectivity. Using insights obtained from crystal structures and MD simulations, we designed lid loop mutants to interrogate the functional significance of lid loop interactions with the gatekeeper tryptophan. We used full-length CRY proteins in order to evaluate the effect of the mutation on the selectivity of KL101 and TH301 since the CCTs are also required for compound selectivity (16). In cell-based degradation assays, a CRY2 F424A mutant displayed a considerably reduced response to TH301 compared with wild-type CRY2 (Fig. 4*A* and *SI Appendix*, Fig. S6*A*), supporting a role of F424 in the stabilization of W417 and its interaction with TH301. In contrast, CRY2 F424A had almost no effect on KL101 response. A neighboring residue CRY2 F423 (corresponding to CRY1 F405) is typically buried in an "auxiliary pocket," composed of F313, F314, A317, F324, I332, M416, and A422 in CRY2, and acts as an anchor to maintain lid loop structure through rigidification of the N-terminal portion (*SI Appendix*, Fig. S7*A*). Because MD simulation of the CRY2-apo W417 "out" model showed that F423 may prevent a W417 "out" conformation by forming a steric clash (*SI Appendix*, Fig. S5*F*), we designed CRY2 F423A and F423A/F424A mutants to potentially reduce interference. The F423A mutant showed a reduced response to TH301, without affecting response to KL101. Interestingly, the F423A/F424A double mutant showed the lowest response to TH301 and a significantly increased response to KL101 (Fig. 4*A* and *SI Appendix*, Fig. S6*A*), resulting in reversed preference of TH301 and KL101. It is likely that the removal of F423 from the auxiliary pocket in the F423A mutant significantly affected the flexibility of the lid loop, but F424 still interacted with an "in" conformation of W417. In contrast, a CRY2 F423A/F424A mutant would gain additional flexibility of the lid loop, enabling W417 to rotate to an "out" position required for a gained KL101 response. We then applied the corresponding mutations to CRY1. A double-mutant F405A/F406A (equivalent to CRY2 F423A/F424A) showed the same response to KL101 and TH301 as wild-type CRY1, while F406A mutant resulted in a blunted response to KL101 (Fig. 4*A* and *SI Appendix*, Fig. S6*A*).

Next, we designed a CRY1 Q407A mutant to perturb a CRY1-specific interaction with the gatekeeper. Compared with the wild type, this mutant showed a dramatically reduced response to KL101 and an increased response to TH301 (Fig. 4*A* and *SI Appendix*, Fig. S6*A*), therefore reversed preference of KL101 and TH301, supporting the role of a W399–Q407 interaction in compound selectivity. A corresponding CRY2 Q425A mutant had an unchanged response to KL101 and an increased response to TH301 compared with the wild type (Fig. 4*A* and *SI Appendix*, Fig. S6*A*). Overall, these data suggest that the lid loop–gatekeeper interactions of CRY1 and CRY2 regulate different responses to KL101 and TH301.

However, because CRY1 F406A showed an unexpectedly reduced response to KL101 even though the residue may not alter gatekeeper conformation, it is also possible that the mutations affect interactions with the CCTs. We therefore investigated the role of the CCTs by swapping them between CRY1 and CRY2. As reported previously (16), both CRY2(PHR)-CRY1(CCT) and CRY1(PHR)-CRY2(CCT) chimeric proteins (designated as CRY2 wild type [WT]-CRY1 CCT and CRY1 [WT]-CRY2 CCT, respectively) showed no response to compounds, indicating that PHRs with CCTs of the same isoform function together to induce selectivity (Fig. 4*B* and *SI Appendix*, Fig. S6*B*). Similar to CRY2 (WT)-CRY1 CCT, CRY2 (F424A)-CRY1 CCT did not respond to KL101 or TH301. In contrast, CRY2 (F423A/F424A)-CRY1 CCT showed a significantly increased response to KL101, resulting in KL101-selective protein similar to CRY1 (WT). Furthermore, CRY2 (Q425A)-CRY1 CCT gained a response to TH301 and became similar to CRY2 (WT) (Fig. 4*B* and *SI Appendix*, Fig. S6*B*). These results in CRY2 lid loop mutants with CRY1 CCT were quite similar to the corresponding CRY2 mutants with their own CCT (Fig. 4*A* and *SI Appendix*, Fig. S6*A*), indicating independence of lid loop mutations from the CCT isoform in determining compound selectivity, and also potential effects of lid loop mutations on CCT interaction.

We further performed assays using CRY1 lid loop mutants with CRY2 CCT. CRY1 (F405A/F406A)-CRY2 CCT was unresponsive to KL101 or TH301, similar to CRY1 (WT)-CRY2 CCT. In contrast, CRY1 (Q407A)-CRY2 CCT and to a lesser extent, CRY1 (F406A)-CRY2 CCT gained response to TH301 similar to CRY2 (WT) (Fig. 4*B* and *SI Appendix*, Fig. S6*B*). The result of CRY1 Q407A mutant with CRY2 CCT correlated well with the corresponding CRY1 mutant with its own CCT (Fig. 4*A* and *SI Appendix*, Fig. S6*A*), again indicating independence of this lid loop mutation from the CCT isoform for compound selectivity. On the other hand, the effects of F406A and F405A/F406A mutations were different between CRY2 CCT- and CRY1 CCT-conjugated CRY1(PHR), suggesting functional interaction of F406 with CCT isoform. Overall, the results demonstrated that lid loop mutation reversed compound selectivity irrespective of CCT isoform, supporting an important role of the lid loop–gatekeeper interaction, although there is also a possibility of lid loop–CCT interaction.

Discussion

We determined crystal structures of CRY2-apo and CRY1-PG4 that identified intrinsically distinct interactions between the gatekeeper tryptophan and lid loop, which were supported by MD simulations. This study provides insight into how structural regulation of the gatekeeper and lid loop can tailor the response of CRY isoforms to small-molecule compounds. The preferential adoption of CRY1 W399 "out" and CRY2 W417 "in" correlated to the conformations observed in crystal structures of isoform-selective compounds: CRY1-KL101, CRY1-KL201, and CRY2-TH301 (16, 26). In contrast, CRY2-selective TH301 caused rotation of the gatekeeper in CRY1, and CRY1-selective KL101 interfered with the gatekeeper in CRY2. In the context of PHR-only constructs, however, these intrinsic gatekeeper conformational differences are not sufficient to confer compound selectivity, although a small degree of preference of KL101 and KL201 for CRY1(PHR) and TH301 for CRY2(PHR) was observed (16, 26). Interactions with the CCTs are required for the selectivity of KL101 for CRY1 and TH301 for CRY2 (16). Because in the *Drosophila* CRY (dCRY) structure (4GU5), the CCT interacts with both W422 (corresponding to the gatekeeper) and the lid loop (31), we propose that similar CCT interactions could occur to stabilize the intrinsic gatekeeper and lid loop conformation for compound selectivity in full-length CRY1 and CRY2. In contrast, the isoform nonselective compound KL001 has a smaller and more flexible methansulfonamide moiety that can be accommodated by intrinsic gatekeeper conformations of CRY1 and CRY2, without incurring steric clashes. A similar mechanism may apply to the nonselective compound KL044, which contains a relatively small chlorobenzonitrile moiety that resides next to the gatekeeper tryptophan (*SI Appendix*, Fig. S4 *B*, *Right*).

A possible caveat of this study is the potential for distal crystal packing to affect the conformation of the region of interest and/or low-frequency modes from the crystal lattice to bias MD simulations. We therefore evaluated the role of lid loop–gatekeeper interactions in compound selectivity by performing cell-based degradation assays with structure-guided mutations of the lid

loop, designed to perturb interactions with the gatekeeper tryptophan. The mutants showed either opposite or different effects on the selectivity of KL101 and TH301 for CRY1 and CRY2, supporting isoform-specific regulatory mechanisms of lid loop–gatekeeper interfaces. CRY1 Q407A designed to disrupt the N–H aryl and H-bond interactions with the gatekeeper almost abrogated response to KL101, while it resulted in gained response to TH301. Similarly, CRY2 F423A/F424A designed to perturb a stacking interaction with the gatekeeper significantly reduced response to TH301 but increased KL101 response. In addition, CRY1 F406A mutant unexpectedly showed a decreased response to KL101, even though F406 did not interact with W399 in CRY1 crystal structures. F406 was orientated in the opposite direction to the FAD pocket, juxtaposed to the C terminus of α22 in the PHR (*SI Appendix*, Fig. S7*B*), and could be accessible to the CCT. Thus, F406A might alter an interaction of the lid loop with the CCT, either directly or through conformational rearrangement. Compared with wild-type CRY1, the basal stability of F406A was slightly reduced, supporting the potential disruption of an interaction (Fig. 4 *A*, *Right*). In contrast, the basal stability of CRY2 was unaffected by F424A. This shows that an equivalent mutation in the lid loops of CRY1 and CRY2 induced distinct effects on stabilization. CCT-swapping experiments showed that PHRs of wild-type CRY1 and CRY2 only exhibit selectivity to KL101 and TH301 compounds in combination with their respective CCTs. Mutations of the lid loop residues (CRY2 F423A/F424A, CRY2 Q425A, and CRY1 Q407A) in CCT-swapped constructs resulted in gain of compound responses, supporting lid loop–CCT interaction. Importantly, however, compound selectivity was determined by lid loop mutation independent of the CCT isoform, indicating the key role of the lid loop–gatekeeper interaction in selective effects. CRY1 F406A with CRY2 CCT resulted in a small gain of TH301 response, also supporting its interaction with the CCT. Similar to F406 in CRY1, Q425 in CRY2 was orientated away from the FAD pocket in the CRY2-apo structure (*SI Appendix*, Fig. S7*B*), indicative of a perturbed interaction with the CCT to affect TH301 response. We propose that the lid loop can regulate compound selectivity by directly interacting with the gatekeeper and the CCT as a potential mechanism that could explain these results.

In addition to the gatekeeper tryptophan and the lid loop, our crystallographic and MD analyses indicated that CRY1 H355, corresponding to CRY2 H373, could favorably adopt distinct conformations. The binding of compounds has been shown to induce conformational changes in this residue (Table 1). H355 in CRY1-KL101 and CRY1-KL201 formed hydrogen bonds with D203-symmetry, and interestingly, a very similar interaction between H355 and D203-symmetry occurred in CRY1-PG4. This intermolecular interaction appeared to mimic an H378–CCT interaction in dCRY (31). Furthermore, the protonation state and position of H378 have been shown to restructure the CCT in dCRY (32), suggesting that corresponding CRY1 H355 potentially interacts with the CCT, depending on its conformation. In CRY1-TH301, the chlorophenyl moiety induced steric restraint of H355 and prevented its interaction with D203-symmetry, resulting in a conformation similar to CRY2 H373. This mechanism possibly perturbs an interaction with the CCT. In the CRY2-TH301 (7EJ9) structure, a different conformation of H377 to CRY2-apo was induced by the proximity of the chlorophenyl group of bound TH301 and also by the repositioning of Y431, possibly due to a shifted lid loop that resulted in a disulfide bond between C430 and C381 (*SI Appendix*, Fig. S5*C*). Because the buffer for protein crystallization contained a high concentration of the reducing agent dithiotheitol (DTT), disulfide bond formation was likely caused by oxidation after the crystals had formed. Interestingly, disulfide bond formation between the corresponding CRY1 residues C412 and C363 has been shown to influence the binding of PER2, which may be regulated by the redox state of the cell (33). This mechanism might also regulate the position of CRY2 H377 and its potential interaction with the CCT, thereby mediating an isoform-selective effect of TH301.

The mechanisms governing differential conformations of the gatekeeper and lid loop in CRY1 and CRY2 need further investigation. Distal effects of variant residues in the PHRs are likely to be involved in affecting the almost identical residues in the FAD pocket and lid loop. Even so, the conformational isomerism between CRY1 and CRY2 described in this study could be exploited for the development of more selective compounds that target distinct gatekeeper tryptophan "out" or "in" conformations with unique structural features of lid loop residues, providing a greater understanding of CRY functions in circadian clock and related diseases.

Materials and Methods

Recombinant CRY Expression and Purification. His_6-MBP-CRY1(PHR) and His_6-MBP-CRY2(PHR) were expressed in Sf9 (*Spodoptera frugiperda*) insect cells. Cell lysates were passed over amylose resin, and fusion proteins were cleaved on the resin with Tobacco Etch Virus (TEV) protease. Cut PHRs were further purified via a HiTrap Heparin HP column before being run on a Superdex 200 10/300 Increase column. CRY1(PHR) and CRY2(PHR) proteins were pooled, buffer exchanged, and concentrated to ∼6.0 mg/mL.

Protein Crystallization and Structure Determination. CRY1(PHR) and CRY2(PHR) were crystallized by hanging-drop vapor diffusion. For CRY1-KL001, CRY1(PHR)-apo crystals were soaked overnight with 0.5 mM KL001. CRY2-TH301 was co-crystallized via hanging-drop vapor diffusion. X-ray diffraction data were collected at Photon Factory or SPring-8 synchrotron facilities. The structures of CRY1-PG4 and CRY1-KL001 were determined using molecular replacement with CRY1-apo structure (6KX4) and CRY2-apo and CRY2-TH301 with CRY2-TH301 structure (6KX8) as search molecules.

MD Simulations. Missing residues were modeled, and PG4 and crystal waters were removed. For CRY1-PG4(removed):KL101 and CRY2-apo:TH301 simulations, KL101 from CRY1-KL101 (6KX6) and TH301 from CRY2-TH301 (6KX8) were superposed and inserted into CRY1-PG4 and CRY2-apo structures, respectively. The resulting complexes were subjected to restrained minimization. Only FAD pocket residues were allowed to move with a restraint on the backbone atoms and no restraint on the side chain atoms. For CRY1-PG4(removed) W399 "in" and CRY2-apo W417 "out" model simulations, the $\chi 2$ torsion angles for CRY1 W399 and CRY2 W417 were changed from −78.8 and 85.6 to 85.7 and −78.9, respectively.

Amber99sb-ildn force field with TIP3P (transferable intermolecular potential with 3 points) water molecules was used for solvation in a dodecahedron box. After neutralization, Na^+ and Cl^- ions were added to maintain an ionic concentration of 0.15 M. Energy minimization followed by equilibration in NVT (constant Number of particles, Volume and Temperature) and NPT (constant Number of particles, Pressure and Temperature) ensemble for 500 ps each was performed for each system. Finally, the data from production runs of 500 ns for CRY1-PG4 and CRY2-apo (three independent runs each); 200 ns for CRY1-PG4(removed):KL101, CRY2-apo:TH301, and CRY2-apo W417 "out"; and 300 ns for CRY1-PG4(removed) W399 "in" were used for analysis. Root mean square fluctuation and dihedral angles were calculated. Interaction energies between residue pairs were calculated by extracting every 1,000th frame from the trajectories of CRY1-PG4 and CRY2-apo and every 100th frame from CRY1-PG4(removed):KL101, CRY2-apo:TH301, CRY1-PG4(removed) W399 "in", and CRY2-apo W417 "out" trajectories.

Thermal Shift Assay. CRY1(PHR) was diluted to 1 μM with DSF (differential scanning fluorimetry) buffer and dispensed onto a 384-well white PCR plate, followed by the application of compounds. SYPRO Orange was added, and thermal denaturation was performed using a real-time PCR detection system.

Degradation Assay. HEK (human embryonic kidney) 293T cells were reverse transfected on a white, solid-bottom 96-well plate with an expression vector for CRY-LUC, its mutant, or LUC. After 24 h, compounds were added to the medium. After 24 h, the medium was supplemented with luciferin and HEPES [4-(2-hydroxyethyl)-1-piperazineethanesulfonic acid]-NaOH. After 1 h, cycloheximide was added, and the luminescence was recorded every 10 min for 18 h. Half-life was obtained by one-phase exponential decay fitting. Relative half-life (CRY-LUC normalized by LUC) at 3.3 μM compound was

obtained by sigmoidal dose–response fitting of dilution series data (five points).

Detailed materials and methods are provided in *SI Appendix, SI Materials and Methods*.

Data Availability. The final coordinates of CRY1-PG4, CRY2-apo, CRY2-TH301, and CRY1-KL001 have been deposited in the PDB (ID codes 7D0M, 7D0N, 7EJ9, and 7DLI). All other study data are included in the article and/or *SI Appendix*.

ACKNOWLEDGMENTS. We thank Natsuko Ono, Dr. Kazuhiro Abe, Dr. Kunio Hirata, Dr. Yusuke Yamada, and Dr. Toshiya Senda for technical assistance. This work was supported in part by Japan Science and Technology Agency Precursory Research for Embryonic Science and Technology Grant JPMJPR14LA; Japan Society for the Promotion of Science Grants 18H02402, 20K21269, and 21H04766; the Takeda Science Foundation; the Uehara Memorial Foundation; the Tokyo Biochemical Research Foundation; and the Hitachi Global Foundation (T.H.). X-ray diffraction data collection and preliminary experiments were carried out at beamlines BL44XU of SPring-8 synchrotron facility (proposals 2017A6743, 2017B6743, 2018B6843, 2019A6942, 2019B6942, and 2020A6542), BL41XU of SPring-8 (proposal 2018B1011), and BL-17A of Photon Factory (proposals 2016R-63, 2017G563, 2019G024, and 2020RP-30). Recombinant CRY expression and beamline experiments were supported in part by Basis for Supporting Innovative Drug Discovery and Life Science Research from Japan Agency for Medical Research and Development support numbers JP20am0101074-0055 and JP20am0101071-0529.

1. J. S. Takahashi, Transcriptional architecture of the mammalian circadian clock. *Nat. Rev. Genet.* **18**, 164–179 (2017).
2. R. P. Aryal *et al*., Macromolecular assemblies of the mammalian circadian clock. *Mol. Cell* **67**, 770–782.e6 (2017).
3. K. Kume *et al*., mCRY1 and mCRY2 are essential components of the negative limb of the circadian clock feedback loop. *Cell* **98**, 193–205 (1999).
4. L. Busino *et al*., SCFFbxl3 controls the oscillation of the circadian clock by directing the degradation of cryptochrome proteins. *Science* **316**, 900–904 (2007).
5. S. I. H. Godinho *et al*., The after-hours mutant reveals a role for Fbxl3 in determining mammalian circadian period. *Science* **316**, 897–900 (2007).
6. S. M. Siepka *et al*., Circadian mutant Overtime reveals F-box protein FBXL3 regulation of cryptochrome and period gene expression. *Cell* **129**, 1011–1023 (2007).
7. A. Hirano *et al*., FBXL21 regulates oscillation of the circadian clock through ubiquitination and stabilization of cryptochromes. *Cell* **152**, 1106–1118 (2013).
8. S.-H. Yoo *et al*., Competing E3 ubiquitin ligases govern circadian periodicity by degradation of CRY in nucleus and cytoplasm. *Cell* **152**, 1091–1105 (2013).
9. N. Koike *et al*., Transcriptional architecture and chromatin landscape of the core circadian clock in mammals. *Science* **338**, 349–354 (2012).
10. A.-L. Huber *et al*., CRY2 and FBXL3 cooperatively degrade c-MYC. *Mol. Cell* **64**, 774–789 (2016).
11. G. T. J. van der Horst *et al*., Mammalian Cry1 and Cry2 are essential for maintenance of circadian rhythms. *Nature* **398**, 627–630 (1999).
12. A. Patke *et al*., Mutation of the human circadian clock gene CRY1 in familial delayed sleep phase disorder. *Cell* **169**, 203–215.e13 (2017).
13. A. Hirano *et al*., A cryptochrome 2 mutation yields advanced sleep phase in humans. *eLife* **5**, e16695 (2016).
14. E. E. Zhang *et al*., Cryptochrome mediates circadian regulation of cAMP signaling and hepatic gluconeogenesis. *Nat. Med.* **16**, 1152–1156 (2010).
15. K. A. Lamia *et al*., Cryptochromes mediate rhythmic repression of the glucocorticoid receptor. *Nature* **480**, 552–556 (2011).
16. S. Miller *et al*., Isoform-selective regulation of mammalian cryptochromes. *Nat. Chem. Biol.* **16**, 676–685 (2020).
17. T. Hirota *et al*., Identification of small molecule activators of cryptochrome. *Science* **337**, 1094–1097 (2012).
18. T. Oshima *et al*., C-H activation generates period-shortening molecules that target cryptochrome in the mammalian circadian clock. *Angew. Chem. Int. Ed. Engl.* **54**, 7193–7197 (2015).
19. J. W. Lee *et al*., Development of small-molecule cryptochrome stabilizer derivatives as modulators of the circadian clock. *ChemMedChem* **10**, 1489–1497 (2015).
20. P. S. Humphries *et al*., Carbazole-containing sulfonamides and sulfamides: Discovery of cryptochrome modulators as antidiabetic agents. *Bioorg. Med. Chem. Lett.* **26**, 757–760 (2016).
21. P. S. Humphries *et al*., Carbazole-containing amides and ureas: Discovery of cryptochrome modulators as antihyperglycemic agents. *Bioorg. Med. Chem. Lett.* **28**, 293–297 (2018).
22. Z. Dong *et al*., Targeting glioblastoma stem cells through disruption of the circadian clock. *Cancer Discov.* **9**, 1556–1573 (2019).
23. A. Czarna *et al*., Structures of *Drosophila* cryptochrome and mouse cryptochrome1 provide insight into circadian function. *Cell* **153**, 1394–1405 (2013).
24. W. Xing *et al*., SCF(FBXL3) ubiquitin ligase targets cryptochromes at their cofactor pocket. *Nature* **496**, 64–68 (2013).
25. S. Nangle, W. Xing, N. Zheng, Crystal structure of mammalian cryptochrome in complex with a small molecule competitor of its ubiquitin ligase. *Cell Res.* **23**, 1417–1419 (2013).
26. S. Miller *et al*., An isoform-selective modulator of cryptochrome 1 regulates circadian rhythms in mammals. *Cell Chem. Biol.* **27**, 1192–1198.e5 (2020).
27. B. R. Crane, Winding down: Selectively drugging a promiscuous pocket in cryptochrome slows circadian rhythms. *Cell Chem. Biol.* **27**, 1109–1111 (2020).
28. A. K. Michael *et al*., Formation of a repressive complex in the mammalian circadian clock is mediated by the secondary pocket of CRY1. *Proc. Natl. Acad. Sci. U.S.A.* **114**, 1560–1565 (2017).
29. K. L. Ode *et al*., Knockout-rescue embryonic stem cell-derived mouse reveals circadian-period control by quality and quantity of CRY1. *Mol. Cell* **65**, 176–190 (2017).
30. J. L. Fribourgh *et al*., Dynamics at the serine loop underlie differential affinity of cryptochromes for CLOCK:BMAL1 to control circadian timing. *eLife* **9**, e55275 (2020).
31. C. Levy *et al*., Updated structure of *Drosophila* cryptochrome. *Nature* **495**, E3–E4 (2013).
32. A. Ganguly *et al*., Changes in active site histidine hydrogen bonding trigger cryptochrome activation. *Proc. Natl. Acad. Sci. U.S.A.* **113**, 10073–10078 (2016).
33. I. Schmalen *et al*., Interaction of circadian clock proteins CRY1 and PER2 is modulated by zinc binding and disulfide bond formation. *Cell* **157**, 1203–1215 (2014).